POTENTIAL FLOW GENERATOR WITH L_2 OPTIMAL TRANSPORT REGULARITY FOR GENERATIVE MODELS

Anonymous authors
Paper under double-blind review

ABSTRACT

We propose a potential flow generator with L_2 optimal transport regularity, which can be easily integrated into a wide range of generative models including different versions of GANs and flow-based models. With up to a slight augmentation of the original generator loss functions, our generator is not only a transport map from the input distribution to the target one, but also the one with minimum L_2 transport cost. We show the correctness and robustness of the potential flow generator in several 2D problems, and illustrate the concept of "proximity" due to the L_2 optimal transport regularity. Subsequently, we demonstrate the effectiveness of the potential flow generator in image translation tasks with unpaired training data from the MNIST dataset and the CelebA dataset.

1 INTRODUCTION

Many of the generative models, for example, generative adversarial networks (GANs) (Goodfellow et al., 2014; Arjovsky et al., 2017; Salimans et al., 2018) and flow-based models (Rezende & Mohamed, 2015; Kingma & Dhariwal, 2018; Chen et al., 2018), aim to find a generator that could map the input distribution to the target distribution.

In many cases, especially when the input distributions are purely noises, the specific maps between input and output are of little importance as long as the generated distributions match the target ones. However, in other cases like image-to-image translations, where both input and target distributions are distributions of images, the generators are required to have additional regularity such that the input individuals are mapped to the "corresponding" outputs in some sense. If paired input-output samples are provided, L_p penalty could be hybridized into generators loss functions to encourage the output individuals fit the ground truth (Isola et al., 2017). For the cases without paired data, a popular approach is to introduce another generator and encourage the two generators to be the inverse maps of each other, as in CycleGANs (Zhu et al., 2017), DualGANs (Yi et al., 2017) and DiscoGANs (Kim et al., 2017), etc. However, such a pair of generators is not unique and lacks clear mathematical interpretation about its effectiveness.

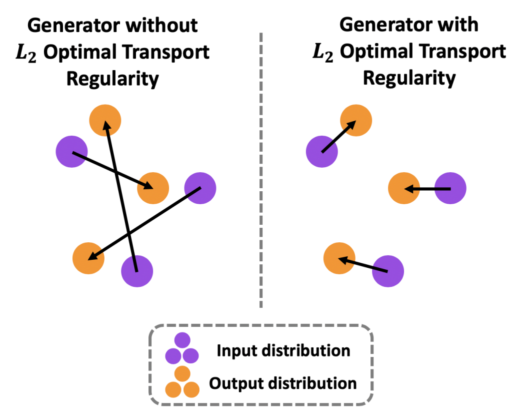

Figure 1: Schematic of generator without and with L_2 optimal transport regularity.

In this paper we introduce a special generator, i.e., the potential flow generator, with L_2 optimal transport regularity. It is not only a map from the input distribution to the target distribution, but also the *optimal transport map* with squared L_2 distance as transport cost. In Figure 1 we provide a schematic comparison between generators with and without optimal transport regularity. While both generators provide a scheme to map from the input distribution to the output distribution, the total squared transport distances in the left generator is larger than that in the right generator. Note that the generator with optimal transport regularity has the characteristic of “proximity”in that the inputs tend to be mapped to nearby outputs. As we will show later, this “proximity” characteristic of L_2 optimal transport regularity could be utilized in image translation tasks. Compared with other approaches like CycleGANs, the L_2 optimal transport regularity has a much clearer mathematical interpretation.

There have been other approaches to learn the optimal transport map in generative models. For example, Seguy et al. (2017) proposed to first learn the regularized optimal transport plan and then the optimal transport map, based on the dual form of regularized optimal transport problem. Also, Yang & Uhler (2018) proposed to learn the unbalanced optimal transport plan in an adversarial way derived from a convex conjugate representation of divergences. In the W2GAN model proposed by Leygonie et al. (2019), the discriminator's objective is the 2-Wasserstein metric so that the generator recovers the L_2 optimal transport map. All the above approaches need to introduce, and are limited to, specific loss functions to train the generators.

Our proposed potential flow generator takes a different approach in that with up to a slight augmentation of the original generator loss functions, our potential flow generator could be integrated into to a wide range of generative models with various generator loss functions, including different versions of GANs and flow-based models. This simple modification makes our method easy to adopt on various tasks considering the existing rich literature and the future developments of generative models.

In Section 2 we give a formal definition of optimal transport map and the motivation to apply L_2 optimal transport regularity to generators. In Section 3 we give a detailed formulation of potential flow generator and the augmentation to the original loss functions. Results are then provided in Section 4. We include a discussion and conclusion in Section 5.

2 Generative Models and Optimal Transport Map

First, we introduce the concept of *push forward*, which will be used extensively in the paper.

Definition 1 *Given two Polish space $\mathbb{X}$ and $\mathbb{Y}$, $\mathcal{B}(\mathbb{X})$ and $\mathcal{B}(\mathbb{Y})$ the Borel σ-algebra on $\mathbb{X}$ and $\mathbb{Y}$, and $\mathcal{P}(\mathbb{X}), \mathcal{P}(\mathbb{Y})$ the set of probability measures on $\mathcal{B}(\mathbb{X})$ and $\mathcal{B}(\mathbb{Y})$. Let $f : \mathbb{X} \to \mathbb{Y}$ be a Borel map, and $\mu \in \mathcal{P}(\mathbb{X})$. We define $f_{\#}\mu \in \mathcal{P}(\mathbb{Y})$, the push forward of μ through f, by*

$$f_{\#}\mu(\mathbb{A}) = \mu(f^{-1}(\mathbb{A})), \forall \mathbb{A} \in \mathcal{B}(\mathbb{Y}). \tag{1}$$

With the concept of push forward, we can formulate the goal of GANs and and flow-based models as to train the generator G such that $G_{\#}\mu$ is equal to or at least close to ν in some sense, where μ and ν are the input and target distribution, respectively. Usually, the loss functions for training the generators are metrics of closeness that vary for different models. For example, in continuous normalizing flows (Chen et al., 2018), such metric of closeness is $D_{\mathrm{KL}}(G_{\#}\mu||\nu)$ or $D_{\mathrm{KL}}(\nu||G_{\#}\mu)$. In Wasserstein GANs (WGANs) (Arjovsky et al., 2017), the metric of closeness is the Wasserstein-1 distance between $G_{\#}\mu$ and ν, which is estimated in a variational form with the discriminator neural network. As a result, the generator and discriminator neural networks are trained in an adversarial way:

$$\min_{G} \max_{D \text{ is 1-Lipschitz}} \mathbb{E}_{\boldsymbol{x}\sim\nu} D(\boldsymbol{x}) - \mathbb{E}_{\boldsymbol{z}\sim\mu} D(G(\boldsymbol{z})), \tag{2}$$

where D is the discriminator neural network and the Lipschitz constraint could be imposed via the gradient penalty (Gulrajani et al., 2017), spectral normalization (Miyato et al., 2018), etc.

Now we introduce the concept of optimal transport map as following:

Definition 2 *Given a cost function $c : \mathbb{X} \times \mathbb{Y} \to \mathbb{R}$, and $\mu \in \mathcal{P}(\mathbb{X})$, $\nu \in \mathcal{P}(\mathbb{Y})$, we let $\mathbb{T}$ be the set of all transport maps from μ to ν, i.e. $\mathbb{T} := \{f : f_{\#}\mu = \nu\}$. Monge's optimal transport problem is to minimize the cost functional $C(f)$ among $\mathbb{T}$, where*

$$C(f) = \mathbb{E}_{\boldsymbol{x}\sim\mu} c(\boldsymbol{x}, f(\boldsymbol{x})) \tag{3}$$

and the minimizer $f^* \in \mathbb{T}$ is called the optimal transport map.

In this paper, we are concerned mostly about the case where $\mathbb{X} = \mathbb{Y} = \mathbb{R}^d$ with L_2 transport cost, i.e., the transport $c(\boldsymbol{x}, \boldsymbol{y}) = \|\boldsymbol{x} - \boldsymbol{y}\|^2$. Also, we assume that μ and ν are absolute continuous w.r.t.

Lebesgue measure, i.e. they have probability density functions. In general, Monge's problem could be ill-posed in that $\mathbb{T}$ could be empty set or there is no minimizer in $\mathbb{T}$. Also, the optimal transport map could be non-unique, for example, if transport cost $c(\boldsymbol{x}, \boldsymbol{y}) = \|\boldsymbol{x} - \boldsymbol{y}\|$. However, for the special case we consider, there exists a unique solution to Monge's problem (Gangbo & McCann, 1996).

Informally speaking, with L_2 transport cost the optimal transport map has the characteristic of "proximity", i.e. the inputs tend to be mapped to nearby outputs. In image translation tasks, such "proximity" characteristic would be helpful if we could properly embed the images into Euclidean space such that our preferred input-output pairs are close to each other. Apart from image translations, the optimal transport problem with L_2 transport cost is important in many other aspects. For example, it is closely related to gradient flow (Ambrosio et al., 2008), Fokker-Planck equations (Santambrogio, 2017), porous medium flow (Otto, 1997), etc.

3 Potential Flow Generator

3.1 Potential Flow Formulation of Optimal Transport Map

We suppose μ and ν have probability density ρ_μ and ρ_ν, respectively, and consider all smooth enough density field $\rho(t, \boldsymbol{x})$ and velocity field $\boldsymbol{v}(t, \boldsymbol{x})$, where $t \in [0, T]$, subject to the continuity equation as well as initial and final conditions

$$\begin{aligned} \partial_t \rho + \nabla \cdot (\rho \boldsymbol{v}) = 0, \\ \rho(0, \cdot) = \rho_\mu, \quad \rho(T, \cdot) = \rho_\nu. \end{aligned} \tag{4}$$

The above equation actually says that such velocity field will induce a transport map: we can construct an ordinary differential equation (ODE)

$$\frac{d\boldsymbol{u}}{dt} = \boldsymbol{v}(t, \boldsymbol{u}), \tag{5}$$

and the map from the initial point to the final point gives the transport map from μ to ν.

As is proposed by Benamou & Brenier (2000), for the transport cost function $c(\boldsymbol{x}, \boldsymbol{y}) = \|\boldsymbol{x} - \boldsymbol{y}\|^2$, the minimal transport cost is equal to the infimum of

$$T \int_{\mathbb{R}^d} \int_0^T \rho(t, \boldsymbol{x}) |\boldsymbol{v}(t, \boldsymbol{x})|^2 d\boldsymbol{x} dt \tag{6}$$

among all $(\rho, \boldsymbol{v})$ satisfying equation (4). The optimality condition is given by

$$\boldsymbol{v}(t, \boldsymbol{x}) = \nabla \phi(t, \boldsymbol{x}), \quad \partial_t \phi + \frac{1}{2} |\nabla \phi|^2 = 0. \tag{7}$$

In other words, the optimal velocity field is actually induced from a flow with time-dependent potential $\phi(t, \boldsymbol{x})$.

3.2 Potential Flow Generator

The potential $\phi(t, \boldsymbol{x})$ is the key function to estimate, since the velocity field could be obtained by taking the gradient of the potential and consequently the transport map could be obtained from Equation 5. There are two strategies to use neural networks to represent ϕ. One can take advantage of the fact that the time-dependent potential field ϕ is actually uniquely determined by its initial condition from Equation 7, and use a neural network to represent the initial condition of ϕ, i.e. $\phi(0, \boldsymbol{x})$, while approximating $\phi(t, \boldsymbol{x})$ via time discretization schemes. Alternatively, one can use a neural network to represent $\phi(t, \boldsymbol{x})$ directly and later apply the PDE regularity for $\phi(t, \boldsymbol{x})$ in Equation 7. We name the generators defined in the above two approaches as *discrete* potential flow generator and *continuous* potential flow generator, respectively, and give a detailed formulation as follows.

3.2.1 Discrete Potential Flow Generator

In the discrete potential flow generator, we use the neural network $\tilde{\phi}_0(\boldsymbol{x}) : \mathbb{R}^d \to \mathbb{R}$ to represent the initial condition of $\phi(t, \boldsymbol{x})$, i.e. $\phi(0, \boldsymbol{x})$. The potential field $\phi(t, \boldsymbol{x})$ as well as the velocity field

$\boldsymbol{v}(t, \boldsymbol{x})$ could then be approximated by different time discretization schemes. As an example, here we use the first-order forward Eular scheme for the simplicity of implementation. To be specific, suppose the time discretization step is Δt and the number of total steps is n with $n\Delta t = T$, then for $i = 0, 1...n$, $\phi(i\Delta t, \boldsymbol{x})$ could be represented by $\tilde{\phi}_i(\boldsymbol{x})$, where

$$\tilde{\phi}_{i+1}(\boldsymbol{x}) = \tilde{\phi}_i(\boldsymbol{x}) - \frac{\Delta t}{2}|\nabla\tilde{\phi}_i(\boldsymbol{x})|^2, \quad \text{for } i = 0, 1, 2..., n-1. \tag{8}$$

Consequently, the velocity field $\boldsymbol{v}(i\Delta t, \boldsymbol{x})$ could be represented by $\tilde{\boldsymbol{v}}_i(\boldsymbol{x})$, where

$$\tilde{\boldsymbol{v}}_i(\boldsymbol{x}) = \nabla\tilde{\phi}_i(\boldsymbol{x}), \quad \text{for } i = 0, 1...n. \tag{9}$$

Finally, we can build the transport map from Equation 5:

$$\begin{aligned} \tilde{\boldsymbol{u}}_0(\boldsymbol{x}) &= \boldsymbol{x}, \\ \tilde{\boldsymbol{u}}_{i+1}(\boldsymbol{x}) &= \tilde{\boldsymbol{u}}_i(\boldsymbol{x}) + \Delta t\tilde{\boldsymbol{v}}_i(\tilde{\boldsymbol{u}}_i(\boldsymbol{x})), \text{ for } i = 0, 1, 2...n-1, \end{aligned} \tag{10}$$

with $G(\cdot) = \tilde{\boldsymbol{u}}_n(\cdot)$ be our transport map.

The discrete potential flow generator has built-in optimal transport regularity since the optimal condition (Equation 7) is encoded in the time discretization (Equation 8). However, such discretization also introduces nested gradients, which dramatically increases computational cost when the number of total steps n is increased. In our practices, we found that even $n = 5$ is almost intractable.

3.2.2 CONTINUOUS POTENTIAL FLOW GENERATOR

In the continuous potential flow generator, we use the neural network $\tilde{\phi}(t, \boldsymbol{x}) : \mathbb{R} \times \mathbb{R}^d \to \mathbb{R}$ to represent $\phi(t, \boldsymbol{x})$. Consequently, the velocity field $\boldsymbol{v}(t, \boldsymbol{x})$ can be represented by $\tilde{\boldsymbol{v}}(t, \boldsymbol{x})$, where

$$\tilde{\boldsymbol{v}}(t, \boldsymbol{x}) = \nabla\tilde{\phi}(t, \boldsymbol{x}). \tag{11}$$

With the velocity field we could estimate the transport map by solving the ODE (Equation 5) using any numerical ODE solver. As an example, we can use the first-order forward Eular scheme, i.e.

$$\begin{aligned} \tilde{\boldsymbol{u}}(0, \boldsymbol{x}) &= \boldsymbol{x}, \\ \tilde{\boldsymbol{u}}((i+1)\Delta t, \boldsymbol{x}) &= \tilde{\boldsymbol{u}}(i\Delta t, \boldsymbol{x}) + \Delta t\tilde{\boldsymbol{v}}(i\Delta t, \tilde{\boldsymbol{u}}(i\Delta t, \boldsymbol{x})), \text{for } i = 0, 1, 2...n-1, \end{aligned} \tag{12}$$

with $G(\cdot) = \tilde{\boldsymbol{u}}(T, \cdot)$ be our transport map, where Δt is the time discretization step and n is the number of total steps with $n\Delta t = T$.

In the continuous potential flow generator, increasing the number of total steps would not introduce high order differentiations, therefore we could have large n, for a better precision of ODE solver. Different from the discrete potential flow generator, the optimal condition (Equation 7) is not encoded in the continuous potential flow generator, therefore we need to penalize Equation 7 in the loss function, as we will discuss in the next subsection.

One may come up with another strategy of imposing the L_2 optimal transport regularity: to use a vanilla generator, which is a neural network directly mapping from inputs to outputs, and penalize the L_2 transport cost, i.e., the loss function is

$$L_{vanilla} = L_{original} + \alpha\mathbb{E}_{x\sim\mu}\|G(\boldsymbol{x}) - \boldsymbol{x}\|^2, \tag{13}$$

where $L_{original}$ is the original loss function for the generator, and α is the weight for the transport penalty. We emphasize that such strategy is much inferior to penalizing Equation 7 in the continuous potential flow generator. When training the vanilla generator with L_2 transport penalty, no matter how we weight the L_2 transport cost penalty, in principle we always have to make a trade off between "matching the generated distribution with the target one" and "reducing the transport cost" since there is always a conflict between them, and consequently $G_{\#}\mu$ will be biased towards μ. On the other hand, there is no conflict between matching the distributions and penalizing Equation 7 in the continuous potential flow generator. As a consequence, the continuous potential flow generator is robust with respect to different weights for the PDE penalty. We will show this in Section 4.

3.3 TRAINING THE POTENTIAL FLOW GENERATOR

While the optimal condition (Equation 7) has been considered in the above two generators, the constraints of initial and final conditions are so far neglected. Actually, the constraint of initial and final conditions gives the principle to train the neural network: we need to tune the parameter in the neural network $\tilde{\phi}$ so that $G_{\#}\mu$ matches ν. This could be done in the fashion of GANs or flow-based models.

3.3.1 LOSS IN GAN MODELS

For the discrete potential flow generator, since the optimal transport regularity is already built in, the loss for training G is simply the GAN loss for the generator, i.e.

$$L_{D-PFG} = L_{GAN}, \tag{14}$$

where L_{GAN} actually depends on the specific version of GANs. For example, if we use WGAN-GP, then $L_{GAN} = -\mathbb{E}_{\boldsymbol{z}\sim\mu} D(G(\boldsymbol{z}))$, where D is the discriminator neural network.

For the continuous potential flow generator, as mentioned above, we also need to make $\tilde{\phi}$ satisify Equation 7 for the optimal transport regularity. Inspired by the applications of neural networks in solving forward and backward problems of PDEs (Lagaris et al., 1998; Raissi et al., 2017a;b; Sirignano & Spiliopoulos, 2018), we penalize the squared residual of the PDE on the so-called "residual" points. In particular, the loss for continuous potential flow generator would be

$$L_{C-PFG} = L_{GAN} + \lambda \frac{1}{N} \sum_{i=1}^{N} [\partial_t \tilde{\phi}(t_i, \boldsymbol{x}_i) + \frac{1}{2} |\nabla \tilde{\phi}(t_i, \boldsymbol{x}_i)|^2]^2, \tag{15}$$

where $\{(t_i, \boldsymbol{x}_i)\}_{i=1}^N$ are the residual points for the estimating the residual of PDE (Equation 7), and λ is the weight for the PDE penalty. While there could be other strategies to select the residual points, here we set them as the points on "trajectories" of input samples, i.e.

$$\{(t_i, \boldsymbol{x}_i)\}_{i=1}^N = \bigcup_{i=0}^{n} \bigcup_{\boldsymbol{x}_j \in \mathbb{B}} \{(i\Delta t, \tilde{\boldsymbol{u}}(i\Delta t, \boldsymbol{x}_j))\}, \tag{16}$$

where $\mathbb{B}$ is the set of batch samples from μ. Note that the coordinates of the residual points involves $\tilde{\boldsymbol{u}}$, but this should not be taken into consideration when calculating the gradient of loss function w.r.t. the generator parameters.

3.3.2 LOSS IN FLOW-BASED MODELS

Our continuous potential flow generator perfectly matches the continuous normalizing flow model proposed by Chen et al. (2018), where the generator is also induced from an ODE. While both density matching and maximum likelihood training could be applied, here we take the latter one as an example: we assume the density of μ and samples from ν are available, and we maximize $\mathbb{E}_{\boldsymbol{y}\sim\nu}[\log p_{G_\#\mu}(\boldsymbol{y})]$, where $p_{G_\#\mu}$ is the density of $G_\#\mu$. Then, the loss for the continuous potential flow generator would be:

$$L_{C-PFG} = -\mathbb{E}_{\boldsymbol{y}\sim\nu}[\log p_{G_\#\mu}(\boldsymbol{y})] + \lambda \frac{1}{N} \sum_{i=1}^{N} [\partial_t \tilde{\phi}(t_i, \boldsymbol{x}_i) + \frac{1}{2} |\nabla \tilde{\phi}(t_i, \boldsymbol{x}_i)|^2]^2, \tag{17}$$

where as in the GAN model, $\{(t_i, \boldsymbol{x}_i)\}_{i=1}^N$ are the residual points for estimating the residual of PDE (Equation 7), and λ is the weight for the PDE penalty. $\mathbb{E}_{y\sim\nu}[\log p_{G_\#\mu}(\boldsymbol{y})]$ could be estimated via the approach introduced in Chen et al. (2018) and we give a detailed description in Appendix B.

The discrete potential flow cannot be trivially applied in flow-based models since we found that the time step size is too large to calculate the density accurately.

4 RESULTS

4.1 2D PROBLEMS

In this subsection, we apply the potential flow generators to several two dimensional problems.

We first study the following two problems where we know analytical solutions for the optimal transport maps. In problem 1 we assume that both μ and ν are Gaussian distributions with $\mu = \mathcal{N}([0;0],[0.25,0;0,1])$ and $\nu = \mathcal{N}([0;0],[1,0;0,0.25])$. In this case the optimal transport map is $f((x,y)) = (2x, 0.5y)$. In problem 2 we assume that μ and ν are concentrated on concentric rings. In polar coordinates, suppose μ has (r,θ) uniformly distributed on $[0.5,1] \times [0,2\pi)$, while ν has

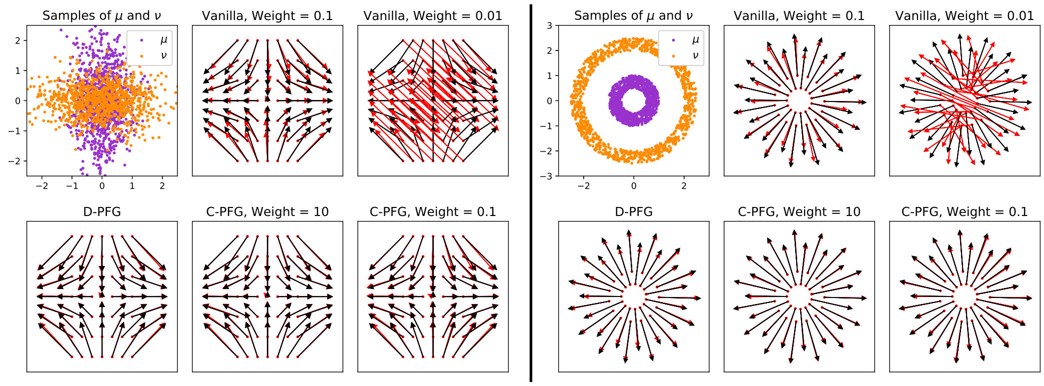

Figure 2: Comparison of different generators: vanilla, discrete potential flow generator (D-PFG), and continuous potential flow generator (C-PFG) in problem 1 (left) and 2 (right). The red arrows represent the map of generators, the black arrows represent the analytical optimal transport map.

Table 1: Comparison of different generators on two problems

	Problem 1			Problem 2	
	Std in x-axis	Std in y-axis	Error of map	Mean of norm	Error of map
Reference	1.000	0.500		2.250	
Vanilla (α=0.1)	0.919±0.004	0.592±0.003	0.108±0.002	2.107±0.002	0.146±0.003
Vanilla (α=0.01)	0.985±0.005	**0.499±0.006**	0.439±0.587	2.227±0.004	0.973±1.319
Vanilla (α=0.001)	0.992±0.009	0.493±0.001	0.462±0.593	2.243±0.002	1.000±1.311
D-PFG	**0.993±0.001**	0.498±0.002	**0.018±0.006**		
C-PFG (λ=10.0)	0.991±0.001	0.502±0.001	**0.018±0.006**	2.243±0.001	**0.024±0.004**
C-PFG (λ=1.0)	0.992±0.001	**0.499±0.002**	0.019±0.007	**2.245±0.000**	0.029±0.002
C-PFG (λ=0.1)	0.990±0.002	0.503±0.003	0.025±0.008	**2.245±0.001**	0.031±0.004

(r, θ) uniformly distributed on $[2, 2.5] \times [0, 2\pi)$, where r and θ are radius and angular, respectively. In this case the optimal transport map is $f((r, \theta)) = (r + 1.5, \theta)$ in polar coordinates. We leave the proofs in Appendix A. Samples from μ and ν as well as the optimal transport map in both problems are illustrated in Figure 2.

For the above two problems we compare the following generators: (a) vanilla generator, i.e., a neural network mapping from $\mathbb{R}^2$ to $\mathbb{R}^2$ to represent the transport map, using loss function in Equation 13 with GAN loss as $L_{original}$, (b) discrete potential flow generator, and (c) continuous potential flow generator with PDE penalty. For the vanilla generator and the continuous potential flow generator, we test different weights for the penalty in order to compare the influences of penalty weights in both generators. As for the GAN loss for generators we use the sliced Wasserstein distance[1], due to its relatively low computational cost, robustness, and clear mathematical interpretation in low dimensional problems (Deshpande et al., 2018). In Figure 2 we illustrate the maps of different generators. A more systematic and quantitative comparison from three independent runs for each case is provided in Table 1, where the best results are marked as bold.

As we already mentioned, the L_2 transport penalty for vanilla generators would make $G_{\#}\mu$ biased towards μ to reduce the transport cost from μ to $G_{\#}\mu$. This is clearly shown in both problems with the penalty weight $\alpha = 0.1$. Actually, we observed more significant biases with larger penalty weights. For the cases with smaller penalty weights $\alpha = 0.01, 0.001$, in some of the runs, while $G_{\#}\mu$ are close to ν, the maps of generators are far from the optimal ones, which shows that the L_2 transport penalty cannot provide sufficient regularity if the penalty weight is too small. These numerical results are consistent with our earlier discussion about the intrinsic limitation of the L_2 transport penalty.

[1]Strictly speaking, there is no "adversarial" training when we use sliced Wasserstein loss since the distance is estimated explicitly rather than represented by an other neural network. However, the idea of computing the distance between fake data and real data coincides with other GANs, especially WGANs. Therefore, in this paper we view sliced Wasserstein distance as a special version of GAN loss.

On the other hand, the potential flow generators give better matching between $G_{\#}\mu$ and ν, as well as smaller errors between the estimated transport maps and the analytical optimal transport maps. Notably, in both problems the continuous potential flow generators give good results with a wide range of PDE penalty weights ranging from 0.1 to 10, which shows the superiority of PDE penalty in the continuous potential flow generators compared with the transport penalty in vanilla generators. We also report that while in the first problem the discrete potential flow generator achieves a comparable result with the continuous potential flow generators, in the second problem we encountered "NAN" problems during training the discrete potential flow generator in some of the runs. This indicates that the discrete potential flow generator is not as robust as the continuous one, which could be attributed to the high order differentiations and small total time steps n in the discrete potential flow generators .

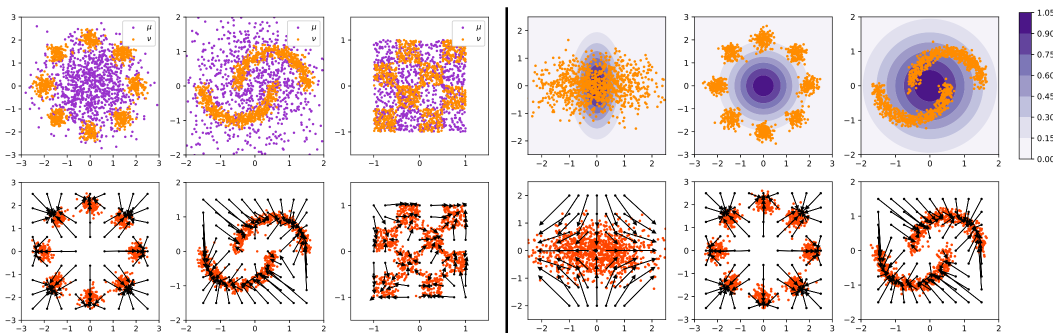

(a) WGAN-GP (b) Continuous normalizing flow

Figure 3: Potential flow generator in (a) WGAN-GP and (b) continuous normalizing flow for different problems. Each column shows the setup and results of one problem. The top row shows the samples or the unnormalized density of μ (purple) and ν (orange), the bottom row shows the map estimated by potential flow generator G and samples of $G_{\#}\mu$.

Apart from the previous two problems, we also applied the continuous potential flow generators with WGAN-GP and continuous normalizing flow models to more complicated distributions, which are illustrated in Figure 3. We can see the match between $G_{\#}\mu$ and ν in each of the problems, as well as that the samples of μ tend to be mapped to nearby positions. This shows the effectiveness of the continuous potential flow generator in various generative models, as well as the characteristics of "proximity" in the potential flow generator maps due to the L_2 optimal transport regularity.

4.2 Image Translations: the MNIST and CelebA dataset

In this section, we aim to show the capability of potential flow generator in dealing with high dimensional problems, and also to show its potential in tasks of image translations using unpaired training data. In particular, we apply the continuous potential flow generator, due to its robustness compared with the discrete potential flow generator, on the following two tasks:

1. Translation between the MNIST images (LeCun et al., 2010). We divide the MNIST training dataset into two clusters: (a) images of digits 0 to 4, and (b) images of digits 5 to 9. We view the two clusters of images as samples of μ and ν, respectively, i.e., we want to find the optimal transport map from images of digits 0 to 4 to images of digits 5 to 9.
2. Translation between the CelebA images (Liu et al., 2015). We randomly pick 60000 images from the CelebA training dataset and divide them into two clusters: (a) images with attribute "smiling" labeled as false, and (b) images with attribute "smiling" labeled as true. The images are cropped so that only faces remain on the images. We view the two clusters as samples of μ and ν, respectively, i.e., we want to find the optimal transport map from no-smiling face images to smiling face images.

Before feeding into the generators, we need to embed the images into a Euclidean space, where the L_2 distances between embedding vectors should quantify the similarities between images. In this paper we apply the principal component analysis (PCA) (Jolliffe, 2011), a simple but highly interpretable approach to conduct the image embedding. The dimensionality of Euclidean space, i.e.

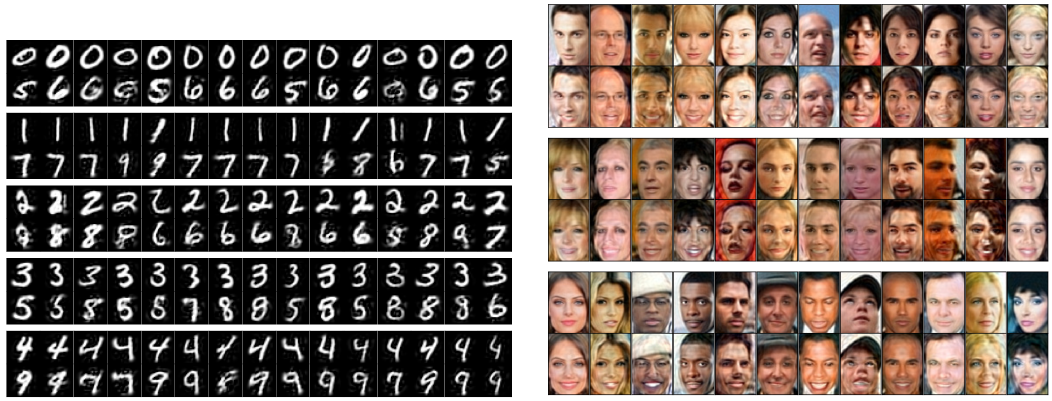

Figure 4: Potential flow generator on the MNIST (left) and CelebA (right) dataset. In each raw, the top images are reconstructed from the input vectors, while the bottom images are reconstructed from the corresponding output vectors.

the total components in PCA, is 100 and 700 for the MNIST and CelebA dataset, respectively. We use WGAN-GP to provide the GAN loss functions in both problems.

In Figure 4 we randomly pick images from the test set and show the corresponding inputs and outputs (more images in Appendix D). On the MNIST dataset, the potential flow generator tends to translate images of digit 0 to digit 6, digit 1 to digit 7, digit 3 to digit 5 or 8, and digit 4 to digit 9. This is consistent with our previous discussion about the characteristics of "proximity" in that the input digits and output digits "look similar", and the corresponding embedding vectors should be close in the L_2 distance. On the CelebA dataset, for most of the images, the potential flow generator could translate the no-smiling faces to smiling faces while keeping the other attributes. We can also see the failure for other images, especially of side faces, which could be partially attributed to the fact that these images are outliers in PCA. The reconstructed output images are blurred, since it's difficult to learn the high order modes of PCA. The results show the effectiveness of L_2 optimal transport map as well as as our potential flow generator in image translation tasks, with clear mathematical interpretation. We think the results are impressive considering that we only use PCA, a linear embedding method, with feedforward neural networks.

5 Conclusions

In this paper we propose potential flow generators with L_2 optimal transport regularity. In particular, we propose two versions: the discrete one and the continuous one. Both could be integrated in GAN models with various generator loss functions, while the latter one could also be integrated into flow-based models. For the discrete potential flow generator, the L_2 optimal transport is directly encoded in, while for the continuous potential flow generator we only need a slight augmentation to the original generator loss functions to impose the L_2 optimal transport regularity.

We first show the correctness of potential flow generators in estimating L_2 optimal transport map by comparing with analytical reference solutions. We report that the continuous potential flow generator outperforms the discrete one in robustness. The continuous potential flow generator is also applied in WGAN-GP and continuous normalizingn flow models, where we illustrated the characteristic of "proximity" for potential flow generator due to L_2 optimal transport regularity. Consequently we show the effectiveness of the potential flow generator in image translation tasks using unpaired training data from the MNIST dataset and the CelebA dataset.

Apart from image-to-image translations, it is also possible to apply the potential flow generator to other translation tasks, if the translation objects could be properly embedded into Euclidean space. Moreover, in this paper we applied PCA for image embedding, and didn't use any convolutional neural networks. A possible improvement is to integrate potential flow generator with other embedding techniques like autoencoders with convolutional neural networks and graph embedding methods, depending on specific tasks. We leave these possible improvements to future work.

REFERENCES

Luigi Ambrosio, Nicola Gigli, and Giuseppe Savaré. *Gradient flows: in metric spaces and in the space of probability measures*. Springer Science & Business Media, 2008.

Martin Arjovsky, Soumith Chintala, and Léon Bottou. Wasserstein generative adversarial networks. In *International Conference on Machine Learning*, pp. 214–223, 2017.

Jean-David Benamou and Yann Brenier. A computational fluid mechanics solution to the monge-kantorovich mass transfer problem. *Numerische Mathematik*, 84(3):375–393, 2000.

Tian Qi Chen, Yulia Rubanova, Jesse Bettencourt, and David K Duvenaud. Neural ordinary differential equations. In *Advances in Neural Information Processing Systems*, pp. 6571–6583, 2018.

Ishan Deshpande, Ziyu Zhang, and Alexander G Schwing. Generative modeling using the sliced Wasserstein distance. In *Proceedings of the IEEE Conference on Computer Vision and Pattern Recognition*, pp. 3483–3491, 2018.

Wilfrid Gangbo and Robert J McCann. The geometry of optimal transportation. *Acta Mathematica*, 177(2):113–161, 1996.

Matthias Gelbrich. On a formula for the L_2 Wasserstein metric between measures on Euclidean and Hilbert spaces. *Mathematische Nachrichten*, 147(1):185–203, 1990.

Ian Goodfellow, Jean Pouget-Abadie, Mehdi Mirza, Bing Xu, David Warde-Farley, Sherjil Ozair, Aaron Courville, and Yoshua Bengio. Generative adversarial nets. In *Advances in Neural Information Processing Systems*, pp. 2672–2680, 2014.

Ishaan Gulrajani, Faruk Ahmed, Martin Arjovsky, Vincent Dumoulin, and Aaron C Courville. Improved training of Wasserstein GANs. In *Advances in Neural Information Processing Systems*, pp. 5767–5777, 2017.

Phillip Isola, Jun-Yan Zhu, Tinghui Zhou, and Alexei A Efros. Image-to-image translation with conditional adversarial networks. In *Proceedings of the IEEE Conference on Computer Vision and Pattern Recognition*, pp. 1125–1134, 2017.

Ian Jolliffe. *Principal component analysis*. Springer, 2011.

Taeksoo Kim, Moonsu Cha, Hyunsoo Kim, Jung Kwon Lee, and Jiwon Kim. Learning to discover cross-domain relations with generative adversarial networks. In *Proceedings of the 34th International Conference on Machine Learning-Volume 70*, pp. 1857–1865. JMLR. org, 2017.

Diederik P Kingma and Jimmy Ba. Adam: A method for stochastic optimization. *arXiv preprint arXiv:1412.6980*, 2014.

Durk P Kingma and Prafulla Dhariwal. Glow: Generative flow with invertible 1x1 convolutions. In *Advances in Neural Information Processing Systems*, pp. 10215–10224, 2018.

Isaac E Lagaris, Aristidis Likas, and Dimitrios I Fotiadis. Artificial neural networks for solving ordinary and partial differential equations. *IEEE transactions on neural networks*, 9(5):987–1000, 1998.

Yann LeCun, Corinna Cortes, and CJ Burges. MNIST handwritten digit database. *ATT Labs [Online]. Available: http://yann. lecun. com/exdb/mnist*, 2, 2010.

Jacob Leygonie, Jennifer She, Amjad Almahairi, Sai Rajeswar, and Aaron Courville. Adversarial computation of optimal transport maps. *arXiv preprint arXiv:1906.09691*, 2019.

Ziwei Liu, Ping Luo, Xiaogang Wang, and Xiaoou Tang. Deep learning face attributes in the wild. In *Proceedings of the IEEE International Conference on Computer Vision*, pp. 3730–3738, 2015.

Andrew L. Maas, Awni Y. Hannun, and Andrew Y. Ng. Rectifier nonlinearities improve neural network acoustic models. In *ICML Workshop on Deep Learning for Audio, Speech and Language Processing*, 2013.

Takeru Miyato, Toshiki Kataoka, Masanori Koyama, and Yuichi Yoshida. Spectral normalization for generative adversarial networks. *arXiv preprint arXiv:1802.05957*, 2018.

Felix Otto. Viscous fingering: an optimal bound on the growth rate of the mixing zone. *SIAM Journal on Applied Mathematics*, 57(4):982–990, 1997.

Maziar Raissi, Paris Perdikaris, and George Em Karniadakis. Physics informed deep learning (part i): Data-driven solutions of nonlinear partial differential equations. *arXiv preprint arXiv:1711.10561*, 2017a.

Maziar Raissi, Paris Perdikaris, and George Em Karniadakis. Physics informed deep learning (part ii): Data-driven discovery of nonlinear partial differential equations. *arXiv preprint arXiv:1711.10566*, 2017b.

Danilo Jimenez Rezende and Shakir Mohamed. Variational inference with normalizing flows. *arXiv preprint arXiv:1505.05770*, 2015.

Tim Salimans, Han Zhang, Alec Radford, and Dimitris Metaxas. Improving GANs using optimal transport. *arXiv preprint arXiv:1803.05573*, 2018.

Filippo Santambrogio. {Euclidean, metric, and Wasserstein} gradient flows: an overview. *Bulletin of Mathematical Sciences*, 7(1):87–154, 2017.

Vivien Seguy, Bharath Bhushan Damodaran, Rémi Flamary, Nicolas Courty, Antoine Rolet, and Mathieu Blondel. Large-scale optimal transport and mapping estimation. *arXiv preprint arXiv:1711.02283*, 2017.

Justin Sirignano and Konstantinos Spiliopoulos. Dgm: A deep learning algorithm for solving partial differential equations. *Journal of Computational Physics*, 375:1339–1364, 2018.

Karren D Yang and Caroline Uhler. Scalable unbalanced optimal transport using generative adversarial networks. *arXiv preprint arXiv:1810.11447*, 2018.

Zili Yi, Hao Zhang, Ping Tan, and Minglun Gong. DualGAN: Unsupervised dual learning for image-to-image translation. In *Proceedings of the IEEE International Conference on Computer Vision*, pp. 2849–2857, 2017.

Jun-Yan Zhu, Taesung Park, Phillip Isola, and Alexei A Efros. Unpaired image-to-image translation using cycle-consistent adversarial networks. In *Proceedings of the IEEE International Conference on Computer Vision*, pp. 2223–2232, 2017.

A PROOF OF THE OPTIMAL MAPS IN SECTION 4.1

In problem 1, for Gaussian distributions μ and ν with mean $\boldsymbol{m}_1$ and $\boldsymbol{m}_2$, as well as covariance matrices $\boldsymbol{\Sigma}_1$ and $\boldsymbol{\Sigma}_2$, from Gelbrich (1990) we know that the minimum transport cost from μ to ν with cost function $c(\boldsymbol{x}, \boldsymbol{y}) = \|\boldsymbol{x} - \boldsymbol{y}\|^2$ is

$$\|\boldsymbol{m}_1 - \boldsymbol{m}_2\|^2 + \mathrm{Tr}(\boldsymbol{\Sigma}_1 + \boldsymbol{\Sigma}_2 - 2(\boldsymbol{\Sigma}_1^{1/2}\boldsymbol{\Sigma}_2\boldsymbol{\Sigma}_1^{1/2})^{1/2}), \tag{18}$$

which is known as the squared Wasserstein-2 distance between two Gaussian distributions. In particular, the minimum transport cost is 0.5 in our problem.

For the map $f((x, y)) = (2x, 0.5y)$, $f_{\#}\mu$ is Gaussian since f is linear. By checking the mean and covariance we have $f_{\#}\mu = \nu$. Also, the transport map of f is

$$\mathbb{E}_{x\sim\mathcal{N}(0,0.25)}(2x - x)^2 + \mathbb{E}_{y\sim\mathcal{N}(0,1)}(0.5y - y)^2 = 0.25 + 0.25 = 0.5 \tag{19}$$

which is exactly the minimum transport cost, thus f is the optimal transport map. We complete the proof of the optimal transport map in problem 1.

In problem 2, denote $\mathbb{X} = [0.5, 1]$, $\mathbb{Y} = [2, 2.5]$, $\mathbb{O} = [0, 2\pi)$, and $m_1 = \mathcal{U}(\mathbb{X})$, $m_2 = \mathcal{U}(\mathbb{Y})$, $m_\theta = \mathcal{U}(\mathbb{O})$, where we use $\mathcal{U}(\mathbb{A})$ to represent the uniform probability measure on set $\mathbb{A}$.

For $f((r, \theta)) = (r + 1.5, \theta)$, $\mu = \mathcal{U}(\mathbb{X}) \times \mathcal{U}(\mathbb{O})$, $\nu = \mathcal{U}(\mathbb{Y}) \times \mathcal{U}(\mathbb{O})$, we have $f_{\#}\mu = \nu$. For any transport map from μ to ν, denote as $g((r, \theta)) = (g_r(r, \theta), g_\theta(r, \theta))$ in polar coordinates, we only need to show that the transport cost of g is no less than the cost of f.

Let $h((r, \theta)) = (g_r(r, \theta), \theta)$, then the transport cost of g is no less than the cost of h since the transport cost is reduced for any point (r, θ).[2]

Actually we could view $g_r(r, \theta)$ as a multivalued function in r so that $g_r(r, \theta)$ induces a transport *plan* H from m_1 to m_2. More formally, define measure $H : \mathcal{B}(\mathbb{X} \times \mathbb{Y}) \to \mathbb{R}$ by

$$H(\mathbb{A}) = \int_{\mathbb{X}}\int_{\mathbb{Y}} \mathbf{1}_{(x,y)\in\mathbb{A}} M(x, dy)dm_1(x) = \int_{\mathbb{A}} M(x, dy)dm_1(x), \tag{20}$$

where $M(\cdot, \cdot) : \mathbb{X} \times \mathcal{B}(\mathbb{Y}) \to \mathbb{R}$ is defined by

$$M(x, \mathbb{A}) = \int_{\mathbb{O}} \mathbf{1}_{g_r(x,\theta)\in\mathbb{A}} dm_\theta(\theta). \tag{21}$$

To see H is a transport plan from m_1 to m_2, we need to check:

1. $\forall \mathbb{A} \in \mathcal{B}(\mathbb{X}), H(\mathbb{A} \times \mathbb{Y}) = m_1(\mathbb{A})$.
   This is true since
   $$H(\mathbb{A} \times \mathbb{Y}) = \int_{\mathbb{A}}\int_{\mathbb{Y}} M(x, dy)dm_1(x) = \int_{\mathbb{A}} M(x, \mathbb{Y})dm_1(x) = m_1(\mathbb{A}), \tag{22}$$
   where we utilize that $M(x, \mathbb{Y}) = 1$.
2. $\forall \mathbb{A} \in \mathcal{B}(\mathbb{Y}), H(\mathbb{X} \times \mathbb{A}) = m_2(\mathbb{A})$.
   Note that $g_{\#}\mu = \nu$, thus $\mu(g^{-1}(\mathbb{A} \times \mathbb{O})) = \nu(A \times \mathbb{O}) = m_2(\mathbb{A})$. Also,
   $$\begin{aligned}\mu(g^{-1}(\mathbb{A} \times \mathbb{O})) &= \int_{\mathbb{X}}\int_{\mathbb{O}} \mathbf{1}_{g(x,\theta)\in\mathbb{A}\times\mathbb{O}} dm_\theta(\theta)dm_1(x) \\ &= \int_{\mathbb{X}}\int_{\mathbb{O}} \mathbf{1}_{g_r(x,\theta)\in\mathbb{A}} dm_\theta(\theta)dm_1(x) \\ &= \int_{\mathbb{X}} M(x, \mathbb{A})dm_1(x) \\ &= H(\mathbb{X} \times \mathbb{A}).\end{aligned} \tag{23}$$
   Therefore $H(\mathbb{X} \times \mathbb{A}) = m_2(\mathbb{A})$.

[2] It's not necessary that $h_{\#}\mu = \nu$.

We also claim that the L_2 transport cost of h equals to that of H. The transport cost of h and H are

$$\begin{aligned} C(h) &= \int_{\mathbb{X}} \int_{\mathbb{O}} (g_r(x,\theta) - x)^2 dm_\theta(\theta) dm_1(x), \\ C(H) &= \int_{\mathbb{X}\times\mathbb{Y}} (y-x)^2 dH = \int_{\mathbb{X}} \int_{\mathbb{Y}} (y-x)^2 M(x,dy) dm_1(x), \end{aligned} \tag{24}$$

respectively. By the definition of M, we have $M(x,\cdot) = g_r(x,\cdot)_{\#} m_\theta$ for any $x \in \mathbb{X}$, thus

$$\int_{\mathbb{Y}} (y-x)^2 M(x,dy) = \int_{\mathbb{O}} (g_r(x,\theta) - x)^2 dm_\theta(\theta) \tag{25}$$

for any $x \in X$. Therefore $C(h) = C(H)$.

Let $F(x) = x + 1.5$ be another transport plan from m_1 to m_2, clearly the L_2 transport cost of f equals to that of F. Note that the transport cost of H is no less than that of F, since the latter one is the optimal transport plan from m_1 to m_2. This complete the proof of claim that the transport cost of g is no less than that of f, and thus the proof of the optimal transport map in problem 2.

B Details of loss functions in continuous normalizing flows

To estimate $\log p_{G_\#\mu}(\boldsymbol{y})$, we have the ODE that connects the probability density at inputs and outputs of the generator:

$$\frac{d}{dt} \log(p(\tilde{\boldsymbol{u}}(t,\boldsymbol{x}))) = -\nabla_{\tilde{\boldsymbol{u}}} \cdot \tilde{v}(t, \tilde{\boldsymbol{u}}(t,\boldsymbol{x})) = -\Delta_{\tilde{\boldsymbol{u}}} \tilde{\phi}(t, \tilde{\boldsymbol{u}}(t,\boldsymbol{x})), \tag{26}$$

for all $\boldsymbol{x}$ in the support of μ, where the initial probability density $p(\tilde{\boldsymbol{u}}(0,\boldsymbol{x})) = p_\mu(\boldsymbol{x})$ is the density of μ at input $\boldsymbol{x}$, while the terminal probability density $p(\tilde{\boldsymbol{u}}(T,\boldsymbol{x})) = p_{G_\#\mu}(G(\boldsymbol{x}))$ is the density of $G_\#\mu$ at output $G(\boldsymbol{x})$.

Also, we estimate $\boldsymbol{x} = G^{-1}(\boldsymbol{y})$ by solving the ODE

$$\frac{d\boldsymbol{w}}{dt} = -\tilde{v}(T-t, \boldsymbol{w}) \tag{27}$$

with initial condition $\boldsymbol{w}(0)$ as $\boldsymbol{y} = G(\boldsymbol{x})$ and $\boldsymbol{w}(T)$ as the corresponding $\boldsymbol{x} = G^{-1}(\boldsymbol{y})$.

For each $\boldsymbol{y}$, we can use Equation 27 to estimate the corresponding $\boldsymbol{x} = G^{-1}(\boldsymbol{y})$, and consequently $\log(p_\mu(\boldsymbol{x}))$ since we have the density of μ. Then we apply Equation 26 to estimate $\log p_{G_\#\mu}(\boldsymbol{y})$. By sampling $\boldsymbol{y} \sim \nu$, we can estimate $\mathbb{E}_{\boldsymbol{y}\sim\nu}[\log p_{G_\#\mu}(\boldsymbol{y})]$. In practice, we also need to discretize Equations 26 and 27 properly. For example, we use the first-order Euler scheme in our practice. Note that when applying maximum likelihood training, the density of μ could be unnormalized, since multiplications with p_μ would merely lead to a constant difference in the loss function.

C Hyperparameters

All the neural networks in this paper are feedforward neural networks of 5 hidden layers, each of width 256 in image translation tasks, or width 128 otherwise. The activation function is $\tanh$ in neural networks for generators and leaky ReLU (Maas et al., 2013) with negative slope 0.2 in discriminator neural networks in WGAN-GP models. We emphasize that we did not use any convolutional neural networks in this paper.

The batch size is set as 1000 for all the cases. We use 1000 random projection directions to estimate the sliced Wasserstein distances. In WGAN-GP model the coefficient for gradient penalty is 0.1, and we do 5 discriminator updates per generator update.

In potential flow generators, the time span T is 1.0. We set the number of total time steps $n = 4$ in discrete potential flow generators, while $n = 100$ in continuous potential flow generators for 2D problems and $n = 10$ in image translation tasks. The PDE penalty weight λ for continuous potential flow generator is set as 1.0 by default, except those in the 2D problems where we compare different generators.

We use the Adam optimizer (Kingma & Ba, 2014) for all the problems. In the 2D problems where we use sliced Wasserstein distance and compare different generators, we set learning rate $l = 10^{-5}$, $\beta_1 = 0.5$, $\beta_2 = 0.999$, and train the generator for $100,000$ steps. In the WGAN-GP model for 2D problems, we set $l = 10^{-5}$, $\beta_1 = 0.5$, $\beta_2 = 0.9$, and train the generator for $100,000$ steps. In the flow-based model we set $l = 10^{-4}$, $\beta_1 = 0.9$, $\beta_2 = 0.999$, and train the generator for $10,000$ steps. In image translation tasks we set $l = 10^{-4}$, $\beta_1 = 0.5$, $\beta_2 = 0.9$, and train the generator for $100,000$ steps.

D MORE RESULTS ON THE MNSIT AND CELEBA DATASET

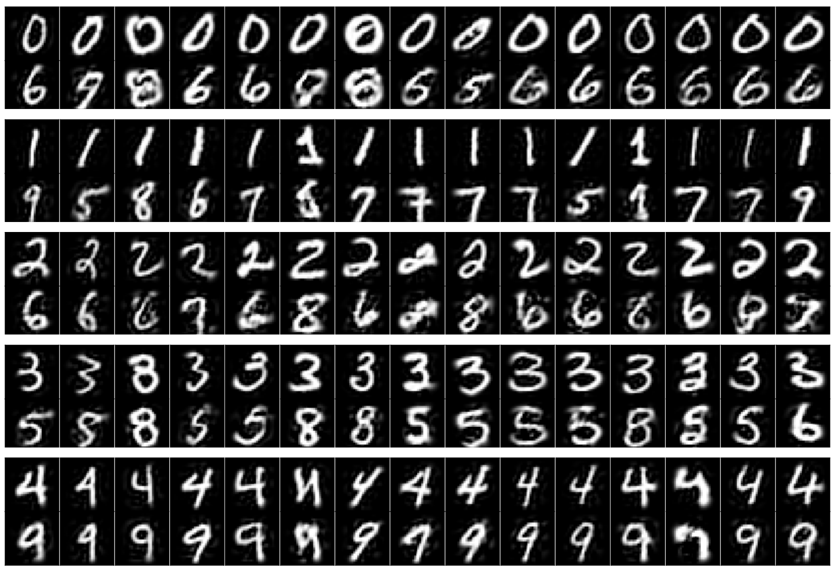

(a) Training dataset

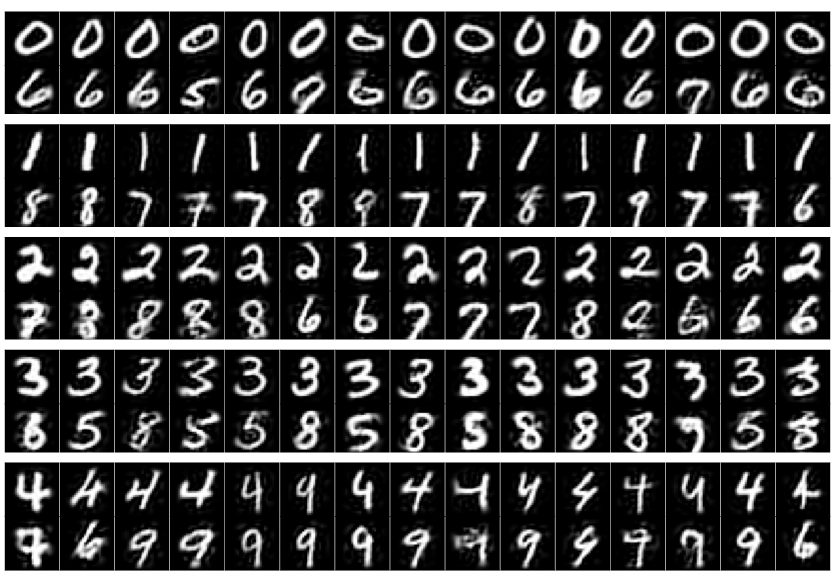

(b) Testing dataset

Figure 5: Potential flow generator on the MNIST (a) training and (b) testing dataset. In each raw, the top images are reconstructed from the input vectors, while the bottom images are reconstructed from the corresponding output vectors.

(a) Training dataset

(b) Testing dataset

Figure 6: Potential flow generator on the CelebA (a) training and (b) testing dataset. In each raw, the top images are reconstructed from the input vectors, while the bottom images are reconstructed from the corresponding output vectors.